JOURNAL OF MATERIALS SCIENCE **36** (2001) 4013–4026

A transmission electron microscopy study of interfaces and matrix homogeneity in ultra-high-performance cement-based materials

L. GATTY, S. BONNAMY
Centre de Recherche sur la Matière Divisée, CNRS and Université d'Orléans, 45071 Orléans cedex 02, France

A. FEYLESSOUFI
Centre de Recherche sur les Matériaux Cimentaires, Université d'Evry – VAL d'Essonne, 91025 Evry cedex, France

C. CLINARD
Centre de Recherche sur la Matière Divisée, CNRS and Université d'Orléans, 45071 Orléans cedex 02, France

P. RICHARD
Centre de Recherche sur les Matériaux Cimentaires, Université d'Evry – VAL d'Essonne, 91025 Evry cedex, France

H. VAN DAMME*
Ecole Supérieure de Physique et Chimie Industrielles, 10 rue Vauquelin, F-75231 PARIS cedex 05, France
E-mail: henri.vandamme@espci.fr

Ultra-high-performance cement-based materials produced under different conditions have been characterized by transmission electron microscopy (TEM), scanning transmission electron Microscopy (STEM), high resolution transmission microscopy (HRTM) and chemical analysis. In addition to cement, these materials contain large amounts of crushed quartz and amorphous submicrometre silica. A post-set heat treatment was also applied in some cases. An abrasive thinning method combined with grazing angle ion etching allowed the preparation of 100 nm thick specimens with wide observation surface areas while avoiding any water or CO_2 contact which may cause changes. Clinker, silica fume and crushed quartz reactivity as a function of the curing processes have been studied, as well as the interfacial zones with the hydrated matrices. The Ca/Si ratio spatial distribution in hydrated products has been analyzed and shown to undergo strong local fluctuations. Nevertheless, the composition fluctuations were less pronounced and the average Ca/Si ratio was lower than in silica-free cement paste. HRTM lattice imaging shows the coexistence of nanocrystalline phases and mesoscale ordered regions within an amorphous matrix. A d-spacings analysis of the nanocrystalline phase suggests a tobermorite-like structure for the calcium silicate hydrates, whereas the mesoscale order might reflect modulations in the water content.

1. Introduction

During the last ten years, considerable advances have been made, in the development of high-performance or more recently ultra-high-performance concretes. Examples include the so-called Densified Small Particles (DSP) materials in which, in addition to cement, small particles have been added in order to densify the cementicious matrix [1–3] and the so-called Reactive Powder Concrete (RPC) materials [4, 5] in which the overall granular formulation and water-to-solids ratio have been further optimized. The design of RPCs, which are in fact microconcretes or mortars, relies on the concomitant improvement of several parameters such as particle-size distribution, porosity and microstructure. Compressive strengths ranging between 200 and 800 MPa, fracture energies between 1200 and 40000 J/m^2 and ultimate tensile strains before fracture of the order of 1% are reached [4, 5]. This was

*Author to whom all correspondence should be addressed.

achieved by reducing the size of the largest aggregates (of the order of 0.5 mm), lowering the water to cement ratio, introducing massive amounts of submicrometre amorphous silica (the so-called silica fume) and, for some special uses, pressing or introducing reactive quartz into the formula. High temperature curing led to further improvement whereas introduction of short metal fibres introduced considerable ductility.

For these materials, the matrix chemical composition, the porosity network morphology and the adhesion of the primary hydrated matrix to silica fume, crushed quartz and clinker particles seem to play an important role. Post-set heat treatments modify the chemical composition of the hydrated products by reducing further their CaO/SiO_2 and H_2O/CaO ratios due to a complementary reaction of some hydrates with silica (the so-called pozzolanic reaction [2]), leading to the formation of tobermorite at temperatures below 200°C and to truscottite, gyrolite, xonotlite and hillebrandite at higher temperatures [6–9]. How these reactions modify the matrix heterogeneity and the interfacial zones between hydrated and non-hydrated products is not yet clear. Even less clear is the mechanism by which they lead to improvement in the mechanical properties of the material but the effect is undoubtedly beneficial in terms of the inhibition of initiation and propagation of microcracks and in a better distribution of the stress field in the matrix.

Recent studies on RPC have analyzed the porosity distribution [8] or the nature and modification of the silicate hydrates due to pressure application during the curing treatment [9]. One important result is that porosity reduction is certainly not the only factor in the enhancement of RPC performance. However, so far, little direct information has been obtained on the micro-, meso- and nanostructure of these materials. Transmission electron microscopy (TEM) with its associated analytical scanning mode (STEM) is a suitable technique, but the relatively small number of published studies on cement pastes and even less on mortars and concretes indicates that its application to cementicious materials is far from obvious [10–20]. This is due to several factors such as difficult sample preparation, sample instability in vacuum and under the electron beam and, ultimately, the poorly defined morphology and crystallinity of the most important matrix material, the calcium silicate hydrate (C–S–H).

Of primary importance for reliable morphological analysis of the microstructure is the quality of the specimen for TEM or STEM observation. This requires thin (less than 100 nm) and, as far as possible, constant thickness specimens over wide observation surface areas (linear size up to several tens of micrometers). This can rarely be achieved with conventional ion etching techniques which produce variable thickness specimens over relatively small surface areas (the walls of the crater produced by the ion beam). In addition, contact with water or CO_2 has to be avoided in order to prevent further hydration or carbonation. As will be described below, an original abrasive preparation method is used in this study which allows the desired specimen features to be achieved.

In this paper, as a function of a qualitative analysis of the reactivity of silica fume, non-hydrated clinker and crushed quartz the curing processes will be presented. Special attention will be paid to the interfacial zone between hydrated products and the other components. In addition, the homogeneity of the hydrated matrix will be semi-quantitatively characterized by measuring the fluctuations in the Ca/Si ratio. Finally, crystallinity and nano- or mesoscale order in the hydrated matrix will be probed by high resolution transmission microscopy (HRTM) lattice imaging.

2. Materials and methods

2.1. Materials

The reference Ultra-High-Performance Concrete (UHPC) considered here, is a RPC type material and was prepared from the following components (mass ratio with respect to cement): type V Portland cement (HPR grade from Lafarge Co); crushed quartz with an average particle diameter of 10 μm from Sifraco Co (0.3); fine quartz sand, 150-400 μm (1.43); undensified amorphous silica fume from Elkem (940 UP grade) with a nitrogen BET surface area of 18 m^2/g (0.325); polymelamine superplasticizer (Superplast from Chryso) (0.055); steel fibres of length 12 mm and diameter 50 μm (0.22); water (0.25). The components were mixed, cast and vibrated as for a conventional concrete. Dry concrete powder components are mixed for 3 to 5 minutes, water is added with half of the volume of the superplasticizer and mixed for 3 minutes, the other half of the volume of the superplasticizer is added and mixed for 5 minutes. The cylindrical sample dimensions were 70 mm in diameter and 140 mm long.

2.2. Curing treatments

Three categories of treatment were then considered. The first category was a cold postset treatment in water at 20°C for 28 days (UHPC-1). The second category consists on different mild temperature treatments: a short mild post-set treatment at 90°C for 8 hours in wet air (UHPC-2); a long post-set treatment at 90°C in wet air for 24 hours and air-drying at 90°C for 24 hours, after an axial pressure application of 65 MPa during setting (UHPC-3); and a long post-set treatment at 90°C in wet air for 24 hours and air-drying at 90°C for 24 hours without any pressure application during setting (UHPC-4)). The last category of treatment consists of hot treatments : air drying at 200°C for 8 days (UHPC-5) for one of the specimens and air drying at 250°C for 8 days for the other one (UHPC-6).

2.3. Mechanical property measurements

The compressive strength of each type of material was measured using a Perrier machine and averaged over five samples for each treatment. The dynamic Young's modulus was calculated from sound velocity measurements, using a Grindosonic instrument.

2.4. Specimen preparation for microscopy

As it has been shown previously that sand and steel fibers do not significantly react with the matrix at the cure temperature [21], the TEM and STEM studies were performed on sand- and fiber-free samples. This was essential for the feasibility of the sample preparation. Thus, in the specimen preparation for electron microscopy, fine sand and steel fibres were removed from the formulation, but for the other components, the same mass ratio with respect to cement was retained.

Preliminary attempts to prepare the specimens by more conventional preparation techniques such as ionic etching or ultramicrotomy after resin-embedding demonstrated that these techniques are not suitable for materials like UHPCs. Therefore, the mechanical polishing technique originally developed at IBM-Fishkill was used. This method uses a tripod which maintains the sample at a constant angle with respect to a rotating abrasive surface. The starting sample is a piece of material a few mm thick, taken from the centre of the cylindrical samples described above, glued on to a side-arm of the tripod. Abrasion is performed with diamond papers with grain sizes going from 30 μm at the beginning of the process down to 0.5 μm at the end. At each change of paper, the quality of the polish is checked by optical microscopy.

The polishing process is performed in two steps. In the first stage, the side-arm is held as parallel as possible to the polishing surface. The aim of this first step is not to obtain a thin sample but simply to have a specimen with one flat and smooth face. The sample is then removed and its polished face is glued to the side arm. The second step is then started in the same way as in the first step, but with control of the sample thickness by optical microscopy. When a thickness of 80 μm is reached, the tripod is adjusted so as to have a small angle ($\leq 0.5^\circ$) with respect to the polishing paper surface. This leads finally to a wedge-shaped sample with a thickness of the order of 1 μm at one end and more than 10 μm at the other end. The thick end is used to handle the sample whereas the thin end is etched further by ion etching under grazing angle incidence for a short time (30 min.) in order to reach the thickness required for a good electron transmission. Thus, some ionic etching is still necessary, but its duration is much less extensive than in conventional ionic milling. In addition, the grazing angle, leads to a specimen with almost parallel faces over a wide area (at the scale of the area explored in TEM), which is not at all the situation in conventional etching. Thin and defect-free samples with quasi-parallel faces as large as $15 \times 20\ \mu m^2$ could easily be obtained. In order to avoid microstructural evolution of these thin samples between preparation and observation, they were kept in a water vapour saturated closed vessel containing soda-lime in order to trap carbon dioxide.

The morphological observations were made using a Philips CM20 microscope at 200 kV in bright field TEM mode and the X-ray microanalyses were performed in the STEM mode at a magnification of 10^4 with a beam size of the order of 5 nm. The samples were always kept at liquid nitrogen temperature. Selected area electron diffraction (SAED) patterns and HRTM lattice images in digitized form were obtained with the same instrument, equipped with a Sofretech 1500 low-dose camera. The combination of these three technical features (low temperature, low-dose camera, rapid digitisation) was essential to avoid rapid damage of the sample under the electron beam and to observe the actual structure. For each sample, two types of observations were performed: (i) at low magnification, in order to study the distribution of crushed quartz and clinker particles, their morphology and their interface with the binding matrix; (ii) at higher magnification, for the microtextural examination of the binding matrix, i.e. the hydrates and the silica fume particles.

3. Results : Mechanical properties and microstructural observations

3.1. Mechanical properties

The curing treatments and mechanical properties are summarized in Table 1.

Thus, the compression strength clearly improves with curing temperature. For the long post-set treatment at 90°C, the application of pressure during setting, which removes excess water from the paste, leads to a further increase in compressive strength. However, a decrease of the Young modulus is observed when curing is performed at 200°C and at 250°C.

3.2. Room temperature or mild thermal curing

This type of cure was applied to UHPC-1 (28 days room temperature curing, Fig. 1) and UHPC-2 (curing at 90°C for 8 hours in wet air, Fig. 2). In general, the samples are very similar, suggesting a time-temperature equivalence of the two treatments. The samples appear very compact, without any cracks or decohesions at the quartz grain/hydrated paste or clinker grain/hydrated paste interfaces. The quartz grains exhibit an angular shape with a sharp boundary and no sign of pozzolanic reaction (Figs. 1a and 2). Extinction lines may be detected in all quartz grains (Fig. 1a). These lines, moving as the orientation of the sample is changed under

TABLE I Curing treatment, compressive strength (Rc) and dynamic modulus (E) of the six Ultra-High-Performance Concretes (UHPC). Note that the mechanical tests were performed on samples prepared with complete formulation, including sand and steel fibres, whereas the samples for electron microscopy were sand- and fibre-free (see Section 2)

	T (°C)	curing treatment	applied pressure	Rc (MPa)	E (MPa)
UHPC-1	20	28 days in water	no	170	60
UHPC-2	90	8 hours in wet air	no	190	62
UHPC-3	90	24 hours in wet air 24 hours in dry air	yes	230	65
UHPC-4	90	24 hours in wet air 24 hours in dry air	no	205	69
UHPC-5	200	8 days in dry air	no	280	50
UHPC-6	250	8 days in dry air	no	310	45

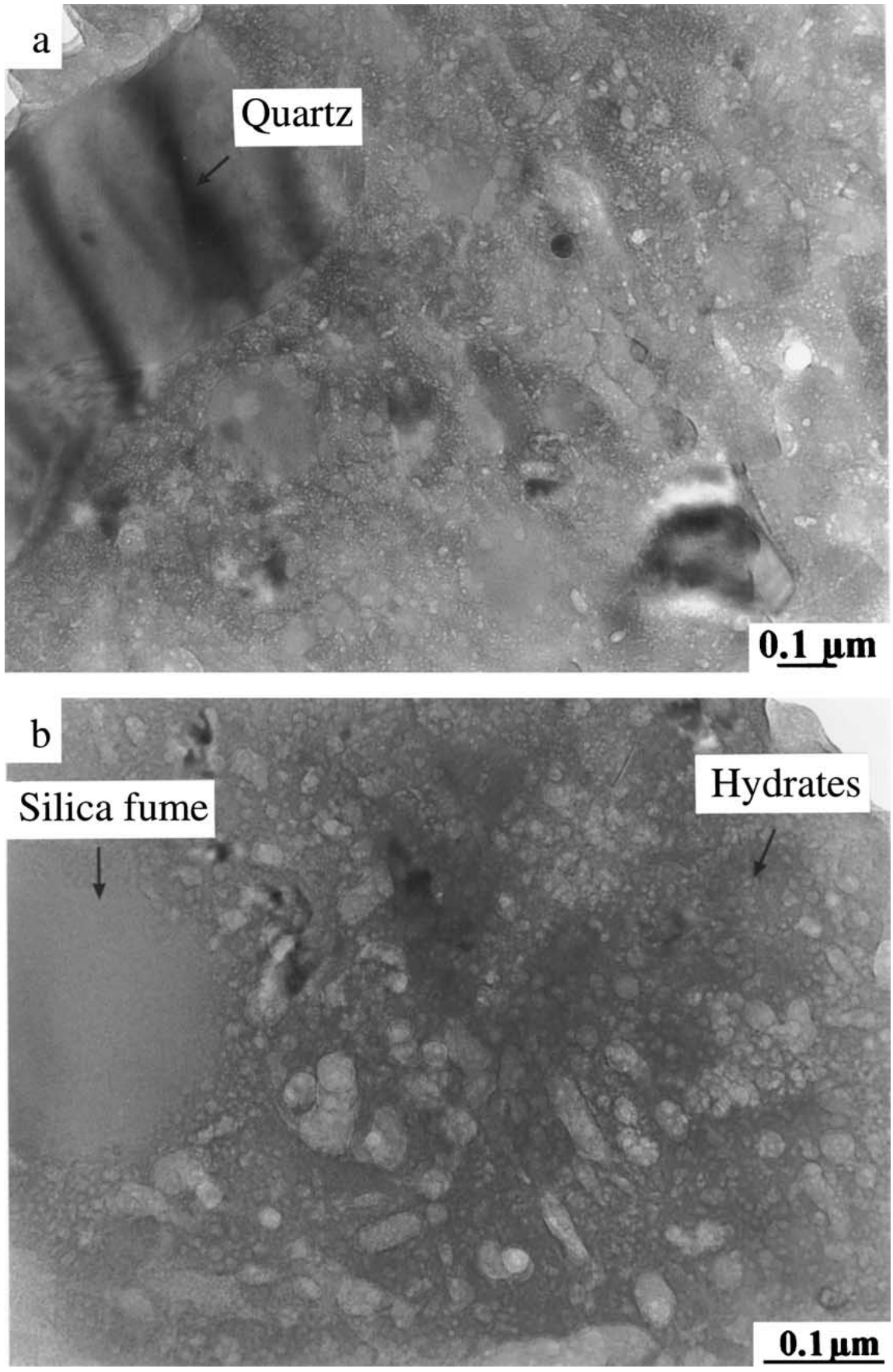

Figure 1 Bright field TEM images of UHPC-1 after room temperature (20°C) curing, showing the quartz and clinker grains (a) and the silica fume particles and the granular microtexture of the hydrated paste (b).

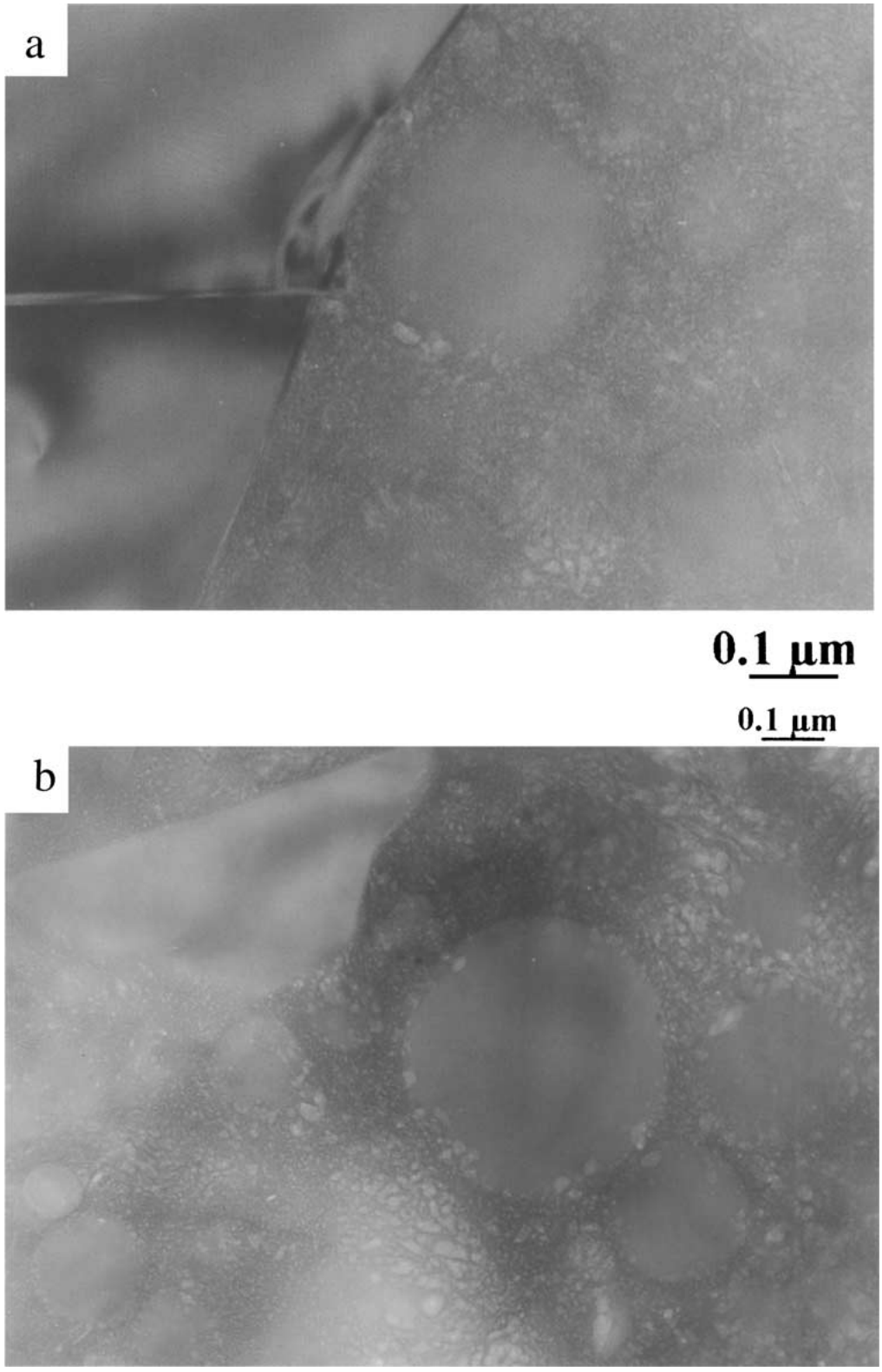

Figure 2 Bright field TEM images of UHPC-2 after mild curing (8 hours at 90°C), showing the sharp quartz-hydrated paste interface and the numerous intact silica fume spheres in the hydrated paste.

the electron beam, are due to the orientation of some crystalline planes under Bragg incidence. The clinker grains exhibit the same morphological features as the quartz grains: angular shape and sharp interface with the matrix.

The hydrated paste microtexture appears homogeneous at the micrometre scale, but with a granular microtexture due to gray level fluctuations at smaller scale (below 0.1 μm) (Figs. 1b and 2). This granularity is likely to be due to chemical composition fluctuations, as will be shown later. The size of the granular domains exhibits wide variations but most of them are within the 20–60 nm range. The interface between the silica fume particles and the matrix is in some cases already somewhat fuzzy, showing that some pozzolanic reaction has already started.

3.3. Moderate curing treatment

This treatment was applied to UHPC-4, which has been cured at medium temperature (90°C) for a relatively long time (48 hours), without compression (Fig. 3). Most quartz grains exhibit some changes. All the smallest grains have a more rounded shape and their interface with the matrix is less sharp. The largest grains are less modified. The extinction lines have disappeared but all grains now exhibit narrow cracks or scratches.

The clinker grains have been more extensively consumed, as revealed by an interfacial zone of the order of 1 μm (Fig. 3a). The hydrated matrix has a microtexture which appears very similar to that of the UHPC-1 sample, with a granular microtexture at fine scale (compare Fig. 3b with Fig. 1b). The size distribution of the granular domains does not seem to be significantly different from that after room temperature curing. However, the emergence of what seems to be some microporosity may now be detected.

3.4. High temperature curing

UHPC-5 and UHPC-6 have been cured for 8 days at high temperature (200 and 250°C, respectively) and their microstructures are illustrated in Fig. 4 and Fig. 5 (the figures illustrate only UHPC-6 since the evolution is basically the same for the two samples, but has been progressed further in UHPC-6). All grains are now partially consumed. All the quartz grains have lost their angular shape and their interface with the hydrated matrix is diffuse. Their texture is very different from that seen after curing at room temperature (UHPC-1). All extinction lines have disappeared and the grains are very extensively cracked.

The clinker grains have been extensively consumed. The largest (more than 10 μm) grains now have a very irregular interface with a wide interfacial zone whereas the smallest grains (less than 5 μm) are totally consumed and only traces can be detected; for some of them, partial recrystallisation has occurred (Fig. 4a).

The hydrated matrix has the same granulare microtexture as before. However, the highest magnifications (Fig. 5) show that some porosity has been generated by the high temperature treatment. This may stem from the volume contraction accompanying dehydration and is probably the reason for the decrease of the Young moduli at these temperatures (Table I). The degree of pozzolanic reaction is also much more advanced. Most silica fume particles have now lost their spheroidal shape (Fig. 4b).

3.5. Influence of compaction during setting

UHPC-3 was under compression during setting and was cured at 90°C for 48 hours afterwards. The most striking result of compression is very extensive cracking along the quartz/matrix and clinker/matrix interfaces (Fig. 6). The cracks also extend within the matrix. Some quartz grains were looser and removed from the matrix during sample preparation. It should be noted that the cracks were not present before sample preparation. They are produced by the polishing treatment, as a result of the large stresses induced by the compression treatment.

The other noticeable differences due to compression are the following: (i) the quartz grains are less stressed than in UHPC-4 (same cure, but no compression during setting), probably due to stress release by crack opening; (ii) the bulk of the hydrated matrix has a more compact texture than in any other sample, except close to the cracks, where open honeycomb-like textures are observed over a distance of the order of 0.5 μm from the crack wall; (iii) the degree of reaction of the clinker grains (for instance, the white arrow on Fig. 6a) seems also to be less than in UHPC-4, which suggests that densification of the matrix has restricted water movement and the extent of pozzolanic reaction during curing.

3.6. Hydrate composition fluctuations

Several analyses were performed along straight lines within the binding matrix containing the hydrates and the silica fume. The analysis spots were separated by about 0.3 μm. Fig. 7 illustrates the UHPC-4 sample after microanalysis. In spite of sample cooling at 77°K, each analysis spot is clearly revealed by the damage due to the 100 sec irradiation.

The Ca/Si ratio fluctuations along three cross sections in UHPC-1, UHPC-4 and UHPC-6 are illustrated in Fig. 8. The most important result is that the Ca/Si ratio exhibits very large fluctuations at length scales of the order of a few hundreds of nm in all samples. The amplitude of these fluctuations is to some extent biased by the presence, in some places, of unhydrated particles which may be detected due to their stoichiometric composition (C/S = 0 for quartz, C/S = 2 for dicalcium silicate and C/S = 3 for tricalcium silicate). Between such particles, the composition fluctuations are less pronouced and the Ca/Si ratio oscillates between 1.1 and 0.4. These values are small compared to those usually reported in the literature, even at high silica fume content [17, 19]. The hydrated paste of UHPCs is clearly very Si-rich. In the samples where the pozzolanic reaction is limited (UHPC-1 and UHPC-2), this result may be partially due to integration of unreacted silica fume particles within the analysed volume. However, within the other samples, the observed Ca/Si ratio is much more directly related to the hydrate composition.

The Ca/Si curves of Fig. 8 decrease extremely rapidly within the transition zone between an anhydrous clinker grain (Ca/Si = 3 or Ca/Si = 2) and the hydrated matrix. After less than 3 or 4 further analyses, the Ca/Si ratio has recovered its average value between 1.1 and 0.4. Thus, the transition zone width is of the order of 1 to 1.5 μm, which is of the same order of magnitude as the transition zone seen in some bright field images (Fig. 3a). In addition, it seems that the hydrates at the transition zone/matrix interface are somewhat richer in Si (Ca/Si close to 0.5) than those at a larger distance.

3.7. Hydrate nanocrystallinity and mesoscale order

A HRTM study was performed on one sample series only, i.e. UHPC-4, which is representative of curing

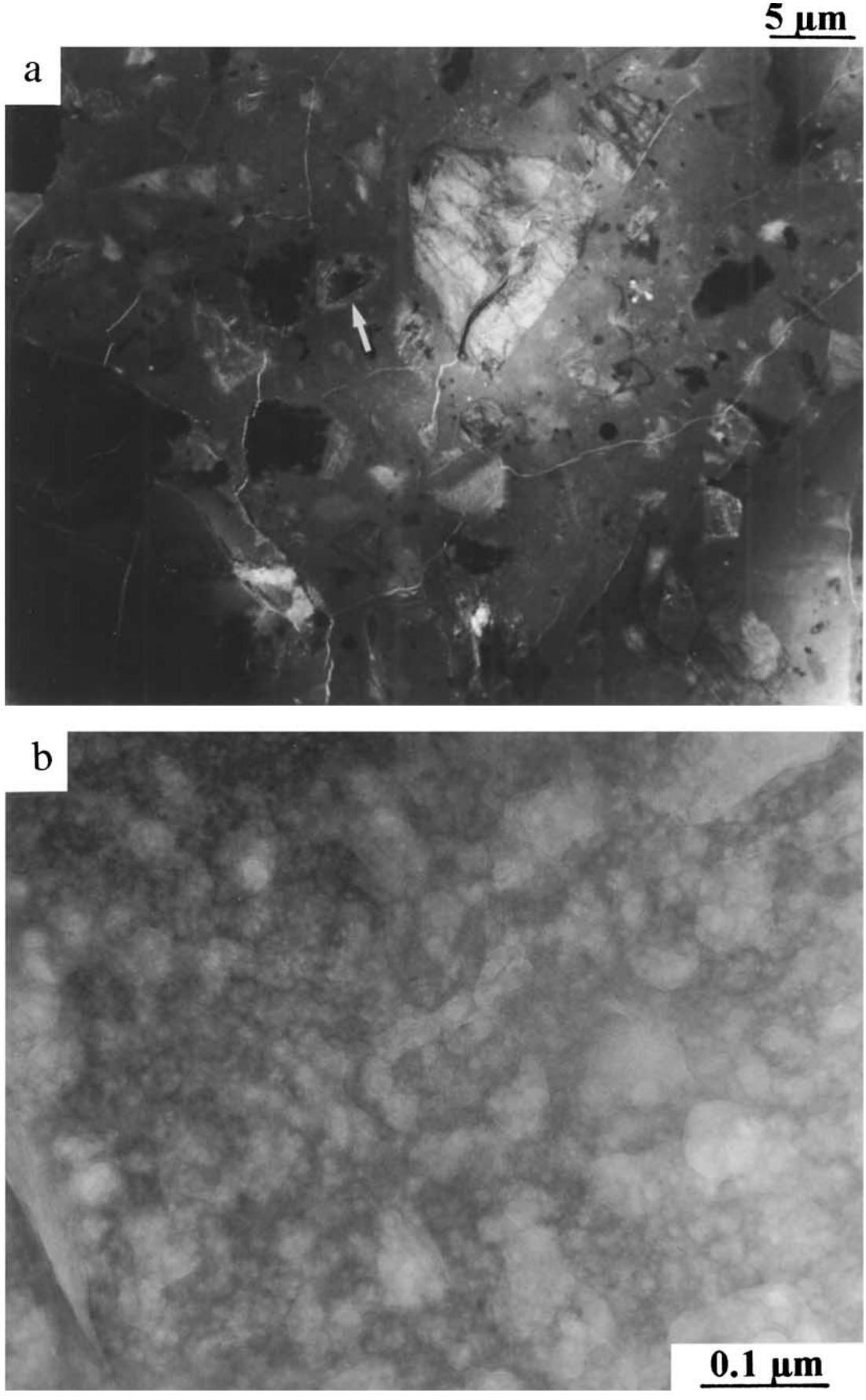

Figure 3 Bright field TEM images of UHPC-4 after long curing at medium temperature (48 hours at 90°C), without compression, showing the appearance of a clinker-paste interfacial zone (white arrow) and the granular character of the hydrated paste.

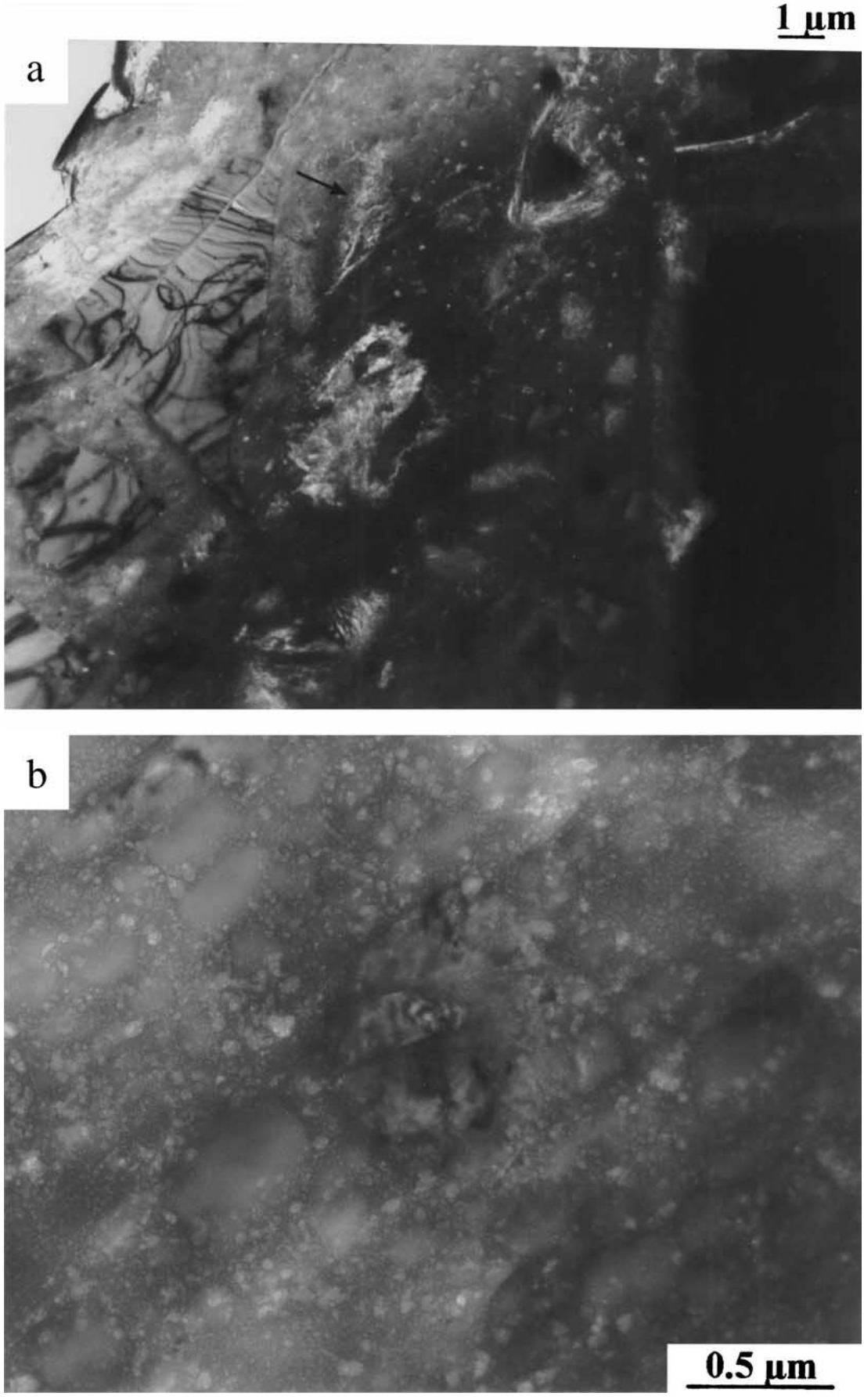

Figure 4 Bright field TEM images of UHPC-6 after long high temperature curing (8 days at 250°C), showing clear signs of reaction of the quartz grains and clinker grains and, in some cases, complete reaction of the clinker grains (black arrow) (a). The influence of the pozzolanic reaction on the silica fume particles surface and shape is also clearly visible (b).

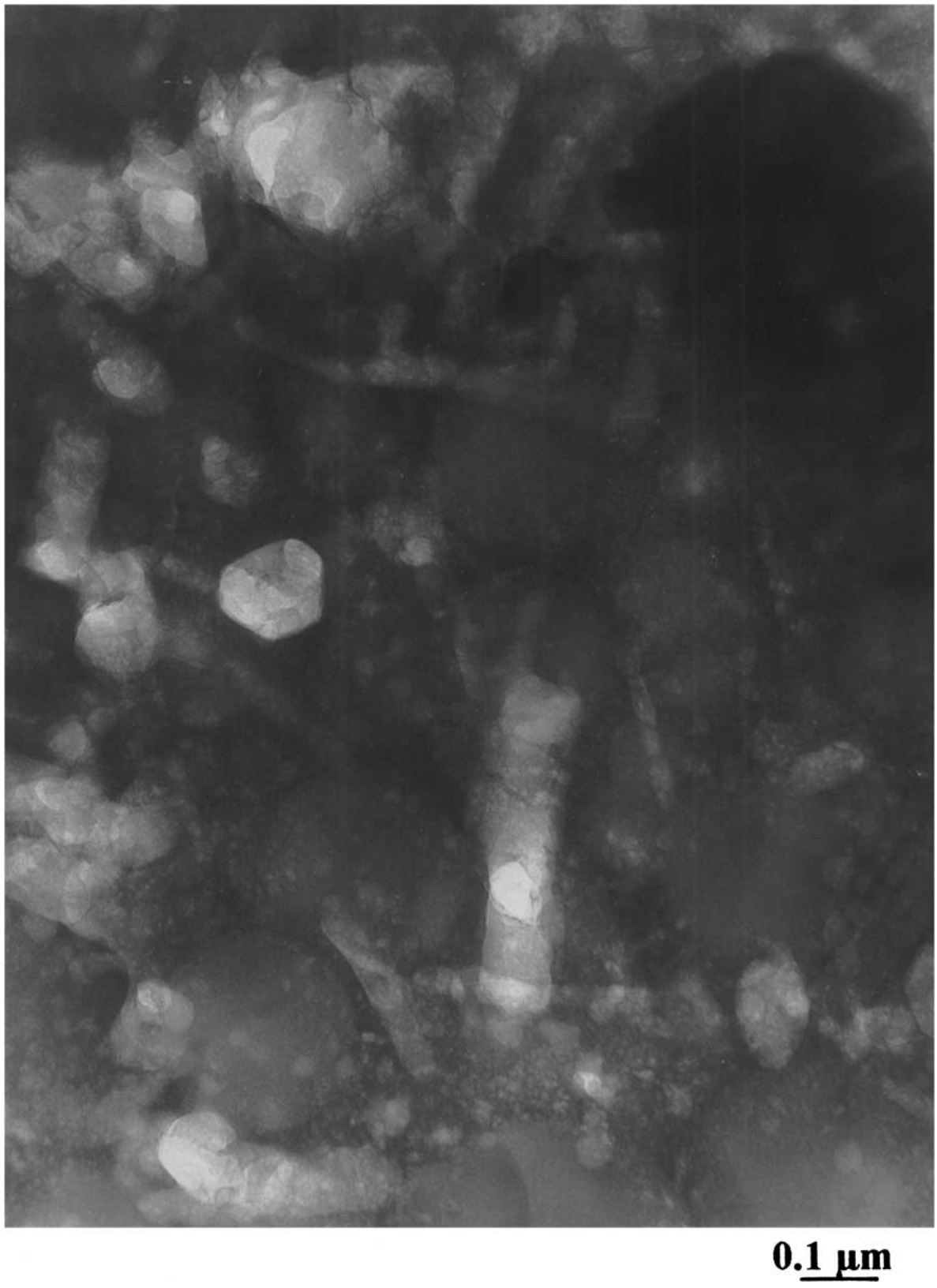

Figure 5 Bright field TEM image High mag UHPC-6 after long high temperature curing (8 days at 250°C), showing the granular microtexture of the matrix and the development of porosity (white zones).

conditions that could be achieved in an industrial context. A typical lattice image of the hydrate gel phase is shown in Fig. 9. In addition to the amorphous matrix background, two types of ordered domains may be observed. The first type of ordered region appears to be nanocrystalline domains. The d-spacing measured on the lattice images (inset of Fig. 9) ranges from 1.136 to 1.380 nm. Unfortunately, these distances could not be detected as diffuse rings in selected area electron diffraction patterns, because they were too close to the central spot. However, such distances are reasonable since they are close to the expected 001 layer periodicity in tobermorite.

The second type of ordered region is more diffuse and is characterized by a much larger scale periodicity. On Fig. 9, it may be estimated at 4 nm, but values

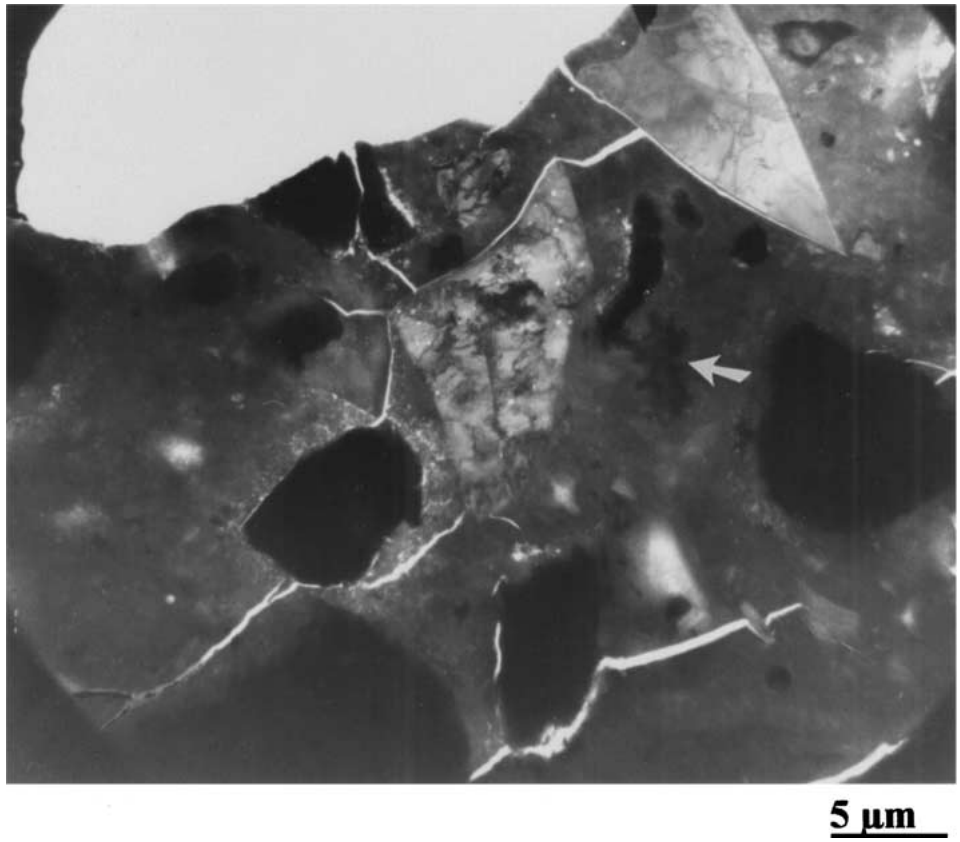

Figure 6 Bright field TEM images of UHPC-3 after long curing at medium temperature (48 hours at 90°C), with compression during setting, showing the extensive cracking along the interfaces induced by the compression treatment. The reactivity of the clinker grain (white arrow) is less pronounced than in the samples that did not undergo compression (Fig. 3a).

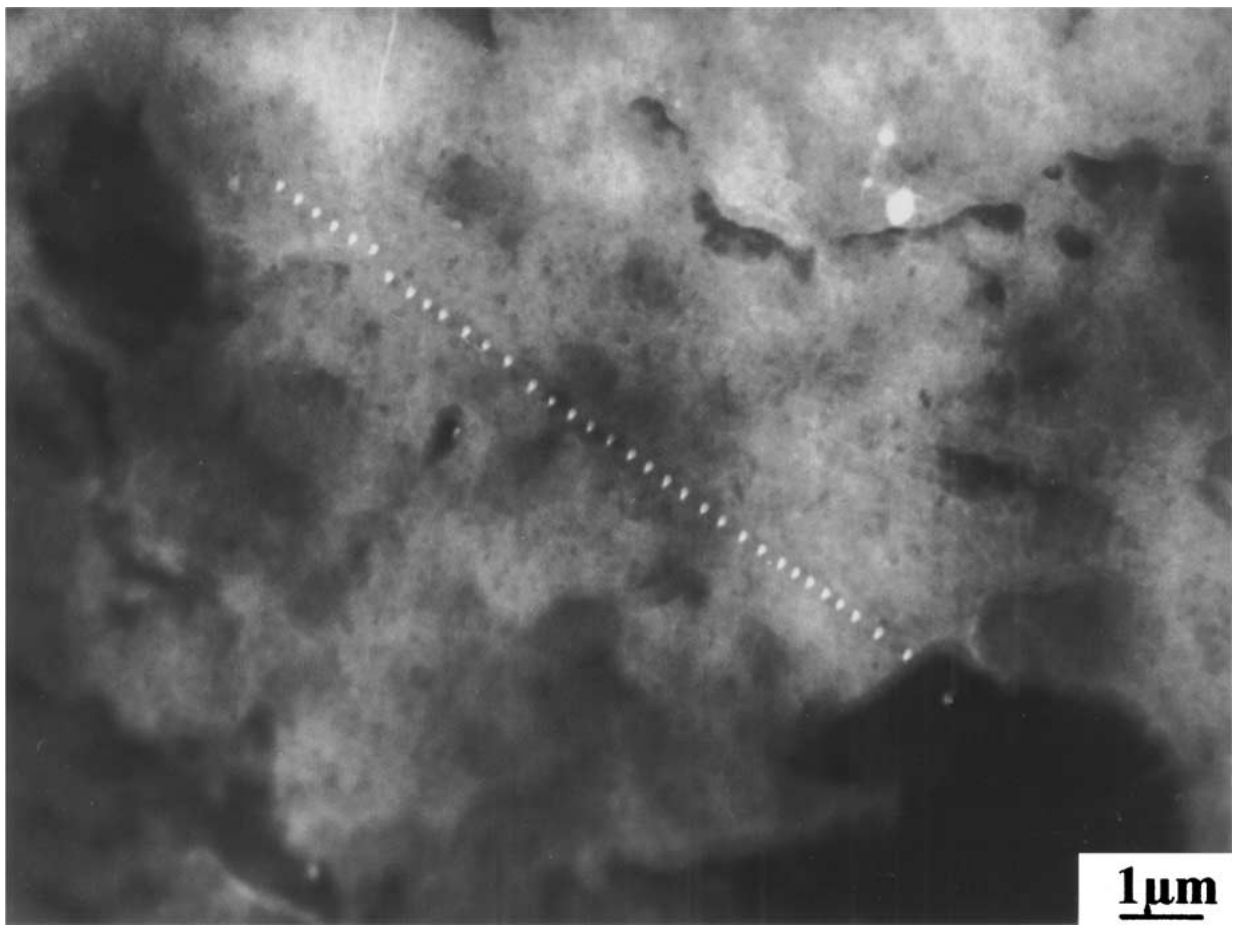

Figure 7 Bright field TEM image of a UHPC-4 sample after microanalysis. The white dots are the trace of the damage left by the X-ray beam.

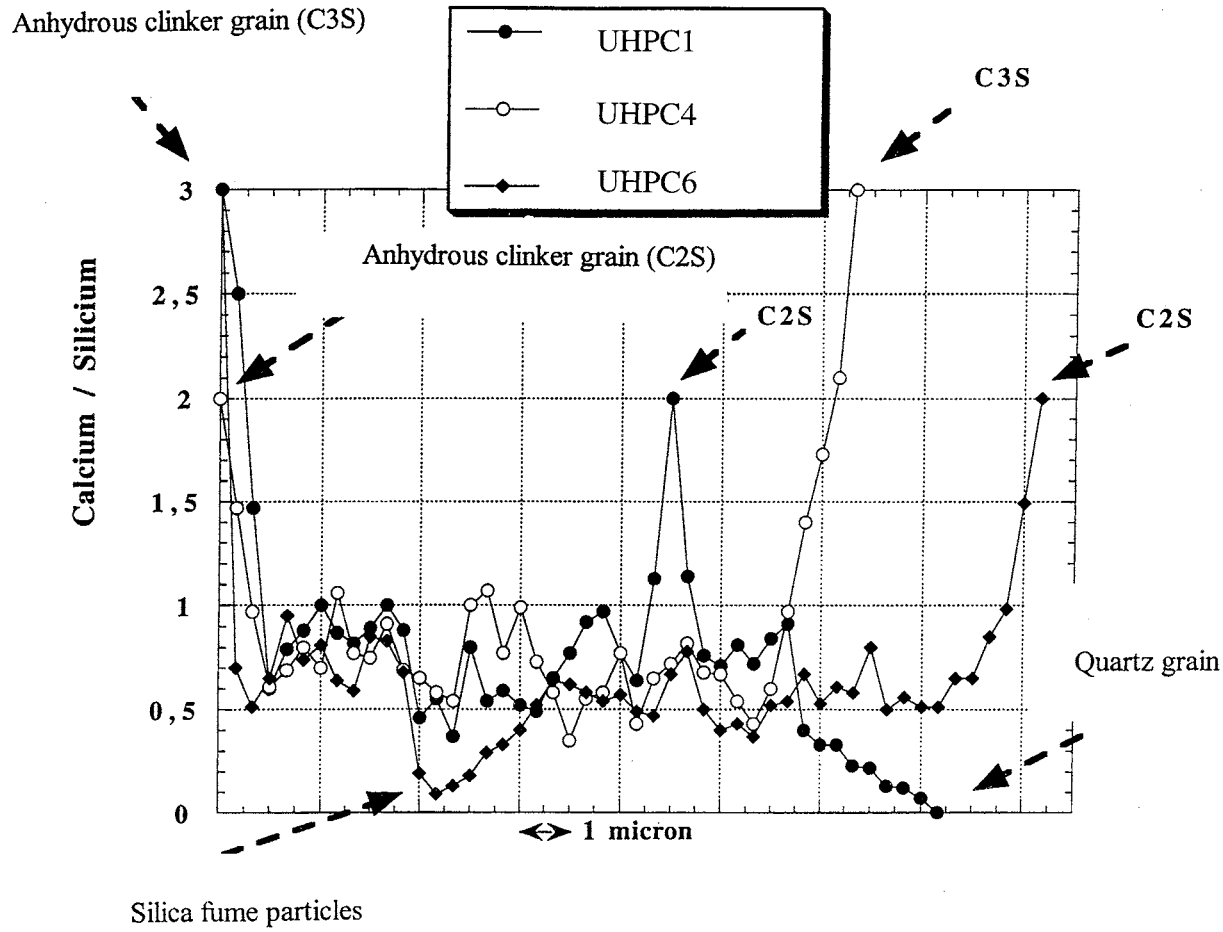

Figure 8 Fluctuations of the Ca/Si ratio along linear cross sections, as obtained by X-ray microanalysis on three UHPC samples UHPC-1 (28 days at 20°C ; UHPC-4 48 hours at 90°C ; 8 days at UHPC-6 250°C). Dicalcium silicate (C2S) and tricalcium silicate (C3S) correspond to a ratio of 2 and 3 respectively.

up to 5 nm were observed. It is not thought that these mesoscale fringes could be assigned to Moiré fringes. This would require the superposition of two perfect regular crystal lattices and the periodicity of the fringes would be much better than what is actually observed. It should be pointed out that this mesoscale ordering is extremely sensitive to the electron beam. It disappears within a few seconds after placing the electron beam on the area, which suggests that it is related to some hydration modulation.

4. Discussion

4.1. Clinker, quartz and silica fume reactivity

These observations confirm clearly that higher curing temperatures improve the compression strength and favour the hydration of unhydrated clinker and the pozzolanic reactivity not only of silica fume (which is a well-documented process, [22]) but also of the fine crushed quartz. The crushed quartz grains may be considered as inert at room temperature, but their pozzolanic reactivity increases dramatically with temperature, as evidenced by: (i) the rounding of their shape which starts in the smallest grains after 48 hours at 90°C and which affects all the grains at 250°C; (ii) the increasingly diffuse character of the quartz/hydrated matrix interface; (iii) the bulk changes to the grains, revealed by the increased cracking, concomitant with the fading away of the extinction lines. This fading is observed on the largest quartz grains starting from 90°C and increases with temperature; (iv) by a complete reaction of the smallest grains, which can be observed after curing at 250°C.

Similarly, increasing the curing temperature enhances hydration of the clinker particles. This is evidenced by the morphological evolution of the grains, by the width of the interfacial zone and, finally, by the complete reaction of the grains, leaving only a "fossil" within the hydrated matrix. This may be interpreted classically [23] as the result of the water evolution from the already formed hydrates, allowing further hydration of the unreacted clinker. Quantitatively, a temperature of the order of 90°C and a duration of more than one day is necessary to obtain a significant effect on the pozzolanic reactivity of quartz and on the secondary hydration of the clinker particles.

Finally, these results provide some evidence that compression during setting, which improves further the mechanical strength, limits the degree of advancement of the chemical reactions (direct clinker hydration and pozzolanic reaction) within the hydrated matrix, probably due to water expulsion and to the higher compactness of the matrix which limits fluid motion.

The decrease of the Young modulus after curing at 200°C and 250°C may seem surprising. A possible explanation lies in the increase of nanoporosity which was observed in these samples, probably stemming from the loss of water from the C–S–H.

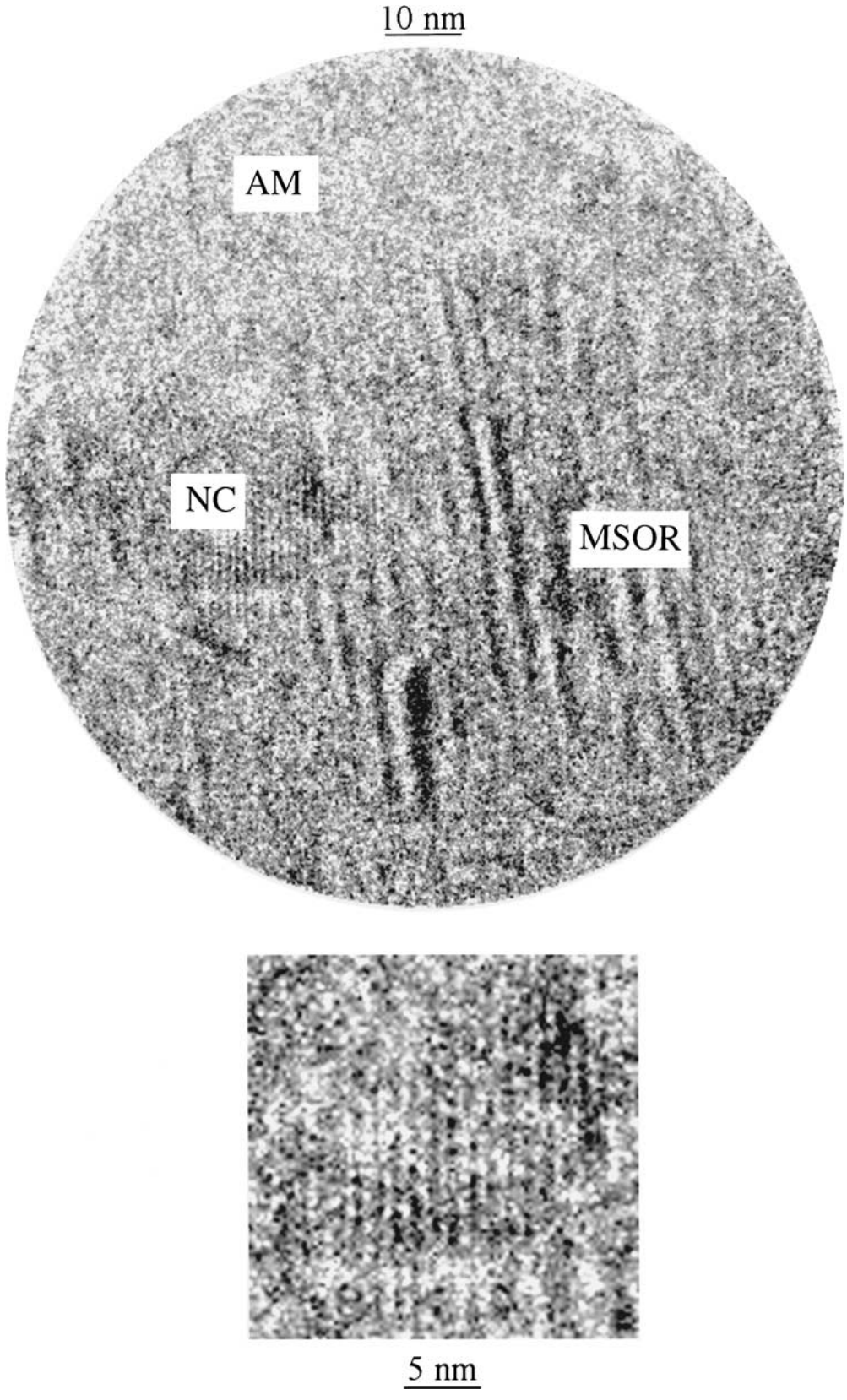

Figure 9 HRTM lattice image of the hydrated paste of a sample after long curing at medium temperature (48 hours at 90°C) showing the amorphous matrix (AM), nanocrystalline zones (NC) and the mesoscale ordered regions (MSOR). The indicated nanocrystalline zone in the upper figure is enlarged below.

4.2. Hydrated matrix structure and composition

As far as the hydrated matrix is concerned, the main observation is that there is basically only one type of hydrate family in this class of high-strength, high-compactness and high silica fume-content materials. Refering to the classical classification scheme for C–S–H [10, 11, 24–27], in which the early hydrates of fibrous or foil-like morphology ("outer products") are distinguished from the more featureless (at μm scale) later-stage hydrates ("inner products"), the hydrates formed in the UHPC investigated here clearly belong

to the second family. The outer product-like morphology was only occasionally observed in the vicinity of the cracks in the compressed sample (UHPC-3). One possible reason for such an homogeneous morphology may be the ubiquitous presence of silica fume particles in very large concentration within the matrix (Fig. 2).

In spite of its homogeneity at μm scale, the hydrated matrix exhibits strong mesoscale heterogeneity. Interestingly, its microtextural heterogeneity (granular texture with gray level domains in the bright field TEM images) and its microanalytical heterogeneity (Ca/Si ratio in STEM mode) are qualitatively comparable. If the analyses which correspond either to pure silica, pure C2S or pure C3S are eliminated then, the Ca/Si ratio fluctuates from ~0.4 to ~1.1, i.e. within a factor of 3 (Fig. 8). This is approximately also the range of fluctuations of the gray level in the hydrated matrix (see Fig. 3b for instance). This qualitative similarity suggests that the microtexture observed in the bright field images is the expression of composition fluctuations.

It may be tempting to associate these fluctuations with the high density of silica fume particles in the original paste, the minima in the Ca/Si ratios indicating the presence of a silica fume particle at that place in the fresh paste. However, this explanation does not hold since even larger fluctuations of the Ca/Si ratio, generally between 0.6 and 2.0, are observed by electron microprobe analysis in the C–S–H gels of neat (silica fume-free) portland cement paste [12, 13, 16, 28, 29]. Recent studies of the mesostructure of C–S–H gels in ordinary portland cement paste (OPC), using the same type of nanoscale analysis as in this work [17, 20], came to the conclusion that the fluctuations were even larger, from 0.5 to 5.9 [17] or from 0.87 to 3.9 [20]. Thus, the noticeable features of the results reported here for UHPC materials is not the existence of large Ca/Si fluctuations but, the opposite, the relatively small amplitude of those fluctuations and the very low mean value, of the order of 0.8. In fact, the very high loading in silica fume seems to *homogenize* the composition of the C–S–H gel.

The size of the domains evidenced in the bright field images deserves some additional comments. Indeed, there is now increasing evidence that the growth of C–S–H leads to the formation of anisotropic "particles" or "domains" with a characteristic lateral size of the order of a few tens of nanometers. In this work, the bright field images reveal a distribution of domain sizes, with an average of the order of 50 nm (see Figs 1b and 3b for instance). This is of the same order as the domain size which was observed by TEM on C–S–H samples prepared by ultramicrotomy (60 nm) [30]. Atomic force microscopy performed on C–S–H layers formed on an amorphous silica surface or on a crystalline C3S (alite) surface in contact with a lime solution [31, 32] also points to the same size (50 nm), but with a narrower distribution. Thus, there appears to be a characteristic length scale associated with C–S–H growth in a variety of conditions, including in complex materials like UHPC.

Finally, though limited, the HRTM study performed on the hydrated matrix after moderate curing (90°C, 48 hours) confirms the general features recently evidenced by Viehland *et al*. [17] and by Zhang *et al*. [20]. In particular, the coexistence of nanocrystalline regions and mesoscale ordered regions, within an amorphous matrix, has been confirmed. Whilst the large d-spacings (from ~1.1 to ~1.4 nm) in the nanocrystalline regions may be easily assigned to the layer stacking in tobermorite-like calcium silicate hydrates, the very large fringes at mesoscale distances (from ~4 to ~5 nm) are more difficult to interpret. Their transient behavior under the electron beam suggests that they might be related to modulations in the local water content.

5. Conclusion

TEM studies of ultra-high performance mortars have been performed. The influence of curing treatment on the reactivity of clinker, quartz and silica fume has been determined and their interfaces with the hydrated matrix have been qualitatively characterized. The high density hydrated matrix has been shown to have the same type of nanostructure as that of ordinary portland cement, with a combination of nanocrystalline regions, mesoscale ordered regions and amorphous matrix. However, the high silica fume content of these materials seems to improve significantly the compositional (Ca:Si ratio) homogeneity of the C–S–H matrix.

Acknowledgements

We thank P-H Albarède from IBM France (Corbeil) for his help in the sample preparation. Ch. Vernet (Bouygues) is gratefully acknowledged for very stimulating discussions. Th. Cacciaguerra (CRMD) is gratefully acknowledged for invaluable technical help.

References

1. P. LU and J. F. YOUNG, *J. Amer. Ceram. Soc*. **76** (1993) 1329.
2. B. BORGLUM, J. F. YOUNG and R. C. BUCHANAN, *Advd. Cem. Bsd. Mater*. **1** (1993) 47.
3. P. LU, G. K. SUN and J. F. YOUNG, *J. Amer. Ceram. Soc*. **76** (1993) 480.
4. P. RICHARD and M. CHEYREZY, in Amer. Concr. Inst. Symposium, ACI Spring Convention, San Francisco (1994) p. 144 and 507.
5. P. RICHARD and M. CHEYREZY, *Cem. Concr. Res*. **25** (1995) 1501.
6. S. A. ABO-EL-ENEIN, E. E. HEKAL, F. I. EL-HOSINY, S. L. MARUSIN, *Il Cemento* **3** (1992) 77.
7. M. DJURIC, M. KOMLJENOVIC, L. PETRASINOVIC-STOJKANOVIC and B. ZIVANOVIC, *Adv. Cem. Res*. **6** (1994) 19.
8. A. FEYLESSOUFI, F. VILLIERAS, L. J. MICHOT, P. DE DONATO, J. M. CASES and P. RICHARD, *Cem. Concr. Composites* **18** (1996) 23.
9. A. FEYLESSOUFI, M. CRESPIN, P. DION, F. BERGAYA, H. VAN DAMME and P. RICHARD, *Advd. Cem. Bsd. Mater*. **6** (1997) 21.
10. A. GRUDEMO, in 4th International Symposium on the Chemistry of Cement, Washington DC, 1962 (US Department of Commerce) p. 615.
11. H. M. JENNINGS, N. J. DALGLEISH and P. L. PRATT, *J. Amer. Ceram. Soc*. **64** (1981) 567.

12. K. MOHAN and H. F. W. TAYLOR, *ibid.* **65** (1982) 717.
13. G. W. GROVES, P. J. LE SUEUR and W. SINCLAIR, *ibid.* **69** (1986) 353.
14. G. W. GROVES, *Mater. Res. Soc. Symp. Proc.* **85** (1987) 3.
15. E. HENDERSON and J. E. BAILEY, *J. Mater. Sci.* **23** (1988) 501.
16. I. G. RICHARDSON and G. W. GROVES, *ibid.* **28** (1993) 265.
17. D. VIEHLAND, J. F. LI, L. J. YUAN and Z. XU, *J. Amer. Ceram. Soc.* **79** (1996) 1731.
18. S. CHATTERJI, *ibid.* **80** (1997) 2959.
19. Z. XU and D. VIEHLAND, *ibid.* **80** (1997) 2961.
20. X. ZHANG, W. CHANG, T. ZHANG and C. K. ONG, *ibid.* **83** (2000) 1731.
21. L. GATTY, Ph.D. thesis, Ecole Centrale de Nantes, Nantes, France, 1996.
22. M. REGOURD, B. MORTUREUX and H. HORNAIN in "Fly Ash, Silica Fume, Slag and Other Mineral By-Products in Concrete," edited by V. M. Malhotra (American Concrete Institute, Detroit, 1983) Vol. 2, p. 847.
23. H. F. W. TAYLOR, *Advd. Cem. Bsd. Mater.* **1** (1993) 38.
24. S. DIAMOND "Hydraulic Cement Pastes: Their Structure and Properties" (Cement and Concrete Association, Slough, U.K., 1976).
25. S. GOTO, M. DAIMON, G. HOSAKA and R. KONDO, *J. Amer. Ceram. Soc.* **59** (1976) 281.
26. P. L. PRATT and A. GHOSE, *Philos. Trans. R. Soc. London* A **310** (1983) 93.
27. K. SCRIVENER and P. L. PRATT, *Mater. Res. Soc. Symp. Proc.* **31** (1984) 351.
28. M. W. GRUTZECK and D. M. ROY, *Nature (London)* **223** (1969) 464.
29. P. L. RAYMENT and A. J. MAJUMDAR, *Cem. Concr. Res.* **12** (1982) 753.
30. R. MAGGION, Ph.D. thesis, Universisté d'Orléans, 1991.
31. S. GAUFFINET, E. FINOT, E. LESNIEWSKA and A. NONAT, *C. R. Acad. Sci. (Paris)* **327** (1998) 231.
32. S. MANSOUTRE, Ph.D. thesis, Université d'Orléans, 1999.

Received 1 September 1999
and accepted 28 March 2001